2021

Seismic behavior of non seismically designed eccentric reinforced concrete beam column joints

Ho Fai Simon Wong

Ying Liu

Pokman Lee

Winghei Kwong

Earthquakes and Structures, *Vol. 21, No. 6 (2021) 613-625*
https://doi.org/10.12989/eas.2021.21.6.613

Seismic behavior of non-seismically designed eccentric reinforced concrete beam-column joints

Ying Liu[1a], Simon H.F. Wong*[1], Hexin Zhang[2b], J.S. Kuang[3c], Pokman Lee[1] and Winghei Kwong[1]

[1]*Faculty of Science and Technology, Technological and Higher Education Institute of Hong Kong, Hong Kong, China*
[2]*School of Engineering and The Built Environment, Edinburgh Napier University Edinburgh, City of Edinburgh, UK*
[3]*Department of Civil and Environmental Engineering, The Hong Kong University of Science and Technology, Hong Kong, China*

(*Received June 16, 2021, Revised August 3, 2021, Accepted August 18, 2021*)

Abstract. Non-seismically designed eccentric reinforced concrete beam-column joints were extensively used in existing reinforced concrete frame buildings, which were found to be vulnerable to seismic action in many incidences. To provide a fundamental understanding of the seismic performance and failure mechanism of the joints, three 2/3-scale exterior beam-column joints with non-seismically designed details were cast and tested under reversed cyclic loads simulating earthquake excitation. In this investigation, particular emphasis was given on the effects of the eccentricity between the centerlines of the beam and the column. It is shown that the eccentricity had significant effects on the damage characteristics, shear strength, and displacement ductility of the specimens. In addition, shear deformation and the strain of joint hoops were found to concentrate on the eccentric face of the joint. The results demonstrated that the specimen with an eccentricity of 1/4 column width failed in a brittle manner with premature joint shear failure, while the other specimens with less or no eccentricity failed in a ductile manner with joint shear failure after beam flexural yielding. Test results are compared with those predicted by three seismic design codes and two non-seismic design codes. In general, the codes do not accurately predict the shear strength of the eccentric joints with non-seismic details.

Keywords: beam-column joint; design codes; eccentricity; seismic behavior; shear strength

1. Introduction

A beam-column joint is one of the key components in typical reinforced concrete (RC) moment-resisting frame structures which are commonly adopted as an important structural system in low or moderate-rise buildings. Beam-column joint transfers internal forces and moments between adjacent columns and beams when the RC frame is subjected to lateral loading. In post-earthquake reconnaissance (Moehle and Mahin 1991, EERI 2001, Kaplan *et al*. 2010), shear failures of RC beam-column joints were observed, which destroyed the mechanism of force transmission and resulted in the collapse of plenty of RC buildings. Over several decades, in order to reduce the seismic risk to existing buildings, a large number of experimental studies have been reported in the literature to investigate the seismic behavior of RC beam-column joints (Lee *et al*. 2009, Mirzabagheri *et al*. 2018, Basha and Fayed 2019, Mogili *et al.* 2019). The test results show that the joints failed due to premature joint shear cracking and reduced energy dissipation because of severe pinching effects. Vanlalruata and Marthong (2021) reports the seismic performance of RC beam-column joint with varying location of construction joints in the column. In addition, with the development of high-performance materials, a large number of experimental and finite element simulation results have been reported that the materials improves the seismic performance of beam column joints (Oinam *et al*. 2019, Raj *et al*. 2020, Halahla *et al*. 2019, Marthong 2019, AI-Osta *et al*. 2020, Karayannis and Golias 2021).

However, the staggering numbers of the existing reinforced concrete building structures built in the low-to-moderate seismic risk regions were mainly designed to resist the service loads which are referred to the wind loads and gravity loads, including dead loads and live loads. The RC beam-column joints of these buildings were traditionally designed without any earthquake resistance details. According to the previous inspections, although there is a geological advantage for the regions of low to moderate seismicity as they are far away from the boundary of the plate, such as the UK, mid-America, Hong Kong and the majority of European countries, it does not mean that the seismic risk is negligible. Deficient beam-column joints designed to older practices and codes often lead to destructive local or global failures.

According to the recent report (GEO 2015), Hong Kong has been shown to be located in the moderate seismicity region, and it is 600 km away from the nearest boundary which is connected to Taiwan, Philippines and Japan. The buildings in Hong Kong were damaged by a 7.42-Magnitude earthquake, which is occurred in Shantou,

*Corresponding author, Associate Professor
E-mail: ceshfw@thei.edu.hk
[a]Research Assistant
E-mail: liuying9208@sina.com
[b]Associate Professor
E-mail: j.zhang@napier.ac.uk
[c]Professor
E-mail: cejkuang@ust.hk

ISSN: 2092-7614 (Print), 2092-7622 (Online)

Guangdong Province in 1918. An earthquake of Magnitude 5.6 occurred in Newcastle, Australia (EERI 1991), where is 1000 km away from the nearest plate boundary. 2.5 billion US dollars of damage was caused by the earthquake occurred in 1991, as the buildings were designed and detailed with only limited seismic resistance. Other typical earthquakes, such as Turkey in 1999, Wenchuan in 2008, have repeatedly demonstrated that the RC beam-column joints without considering seismic resistance details are more vulnerable. The experimental tests of Kwon *et al.* (2012), Choi *et al.* (2017) from Korea and Kuang and Wong (2013) from Hong Kong revealed that the RC beam-column joints with sub-standard details performed poorly under reversed cyclic loads. Lee and Ko (2007) reported the experimental results which show that eccentricity had negative effects on the seismic performance. Nonetheless, only limited results of non-seismically designed eccentric exterior joints have been reported in the literature.

The primary objective of this study is to investigate the effects of eccentricity in joint on the shear strength and hysteretic characteristics of non-seismically detailed exterior beam-column joints subjected to simulated seismic loading caused by a moderate earthquake. In this paper, reversed cyclic-load tests of 2/3-scale eccentric RC exterior beam-column joints, simulating those in as-built RC framed buildings designed to Hong Kong Code of Practice of Structure Use of Concrete 2013 (HKSUC 2013), are presented. In order to evaluate the validity of code-prescribed methods for predicting the shear strength of the joints, the experimental results are compared with three seismic and two pre-seismic design codes, which are widely used and include ACI 318, NZS 3101, Eurocode 8, HKSUC 2013 and Eurocode 2.

2. Experimental programme

2.1 Test specimens

Three 2/3-scale exterior RC beam-column joints with section dimensions 300 mm×300 mm for columns and 150 mm×450 mm for beams are fabricated, as shown in Fig. 1. All specimens, for which the basis of design is based on the Hong Kong Code of Practice of HKSUC 2013, each having the similar material characteristics and the same longitudinal reinforcement details. Each column is reinforced with 4T20 and each beam is reinforced with an equal amount of longitudinal bars of 2T20 at both top and bottom sides of the cross-section. Both tension and compression bars in the beam are bent into the joint. The point of contraflexure is assumed to be in the mid-span of beams and mid-height of columns, respectively, which served as the boundary condition of the specimen under reversed cyclic loading. The thickness of the concrete cover is 25 mm.

Eccentricity is the primary parameter of the investigation, and it is defined as the horizontal distance between the centerline of the beam and the column, as shown in Fig. 1. The eccentricity of 0 mm, 37 mm and 75 mm was investigated in this study, which represents no eccentricity, 1/8 of column width (b_c) eccentricity and b_c/4 eccentricity, respectively.

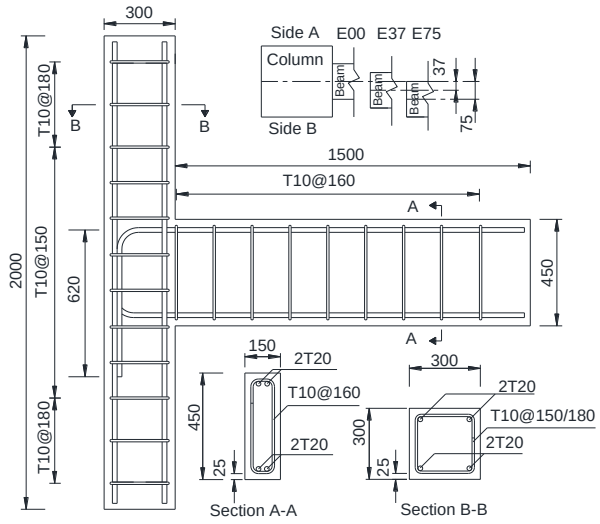

Fig. 1 Reinforcement and geometry details (unit: mm)

Table 1 Material properties

Specimen	E00	E37	E75
Concrete compressive strength, f_{cu} (f'_c)*: MPa	40.1(32.1)	46.8(37.4)	42.3(33.8)

*f_{cu}: The compressive cube strength of concrete; f'_c: The compressive cylinder strength of concrete

A nomenclature system is established for the test specimens to represent its characteristics, so as to make a comparative analysis in the latter part of this paper. The nomenclature system is mainly used to represent the eccentricity. For example, the name E75 of the specimen, which represents that the eccentricity is 75 mm. Specimen E00 was manufactured as a control specimen, and all specimens were tested at least 28 days after the fabrication date (HKSUC 2013).

2.2 Materials

Every specimen was separately constructed in the laboratory and three cubes of 150 mm were cast and cured in the same condition for each specimen. Considering the strength of concrete used in the existing moment-resisting reinforced concrete frames, the average compressive strengths of concrete in this study are summarized in Table 1. High yield reinforcement bars were used in this experimental study with the yield strength, f_y, of 500 MPa, which have high strength and high ductility.

2.3 Test set-up

The experimental set-up and loading system are shown in Fig. 2. For convenience of testing and applying loading, the T-shaped exterior joint specimen was rotated 90 degrees, so that the column was in the horizontal position and the beam was in the vertical position. Proper boundary conditions were provided in the set-up to simulate the actual

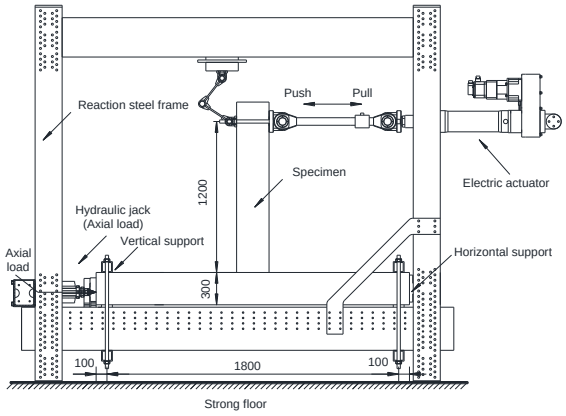

(a) Schematic test set-up

(b) Actual test rig

Fig. 2 Test rig

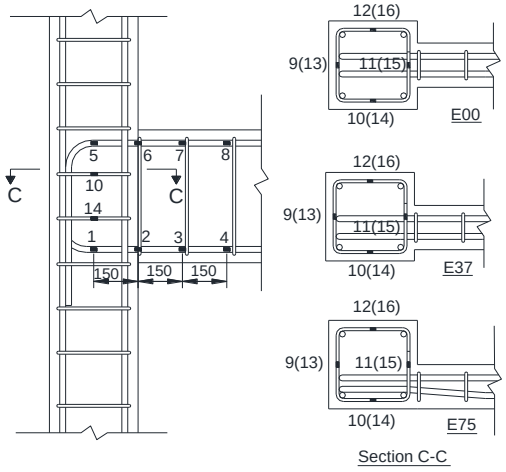

Fig. 3 Position of strain gauges in specimens (number shown in bracket are strain gauge number in lower layer)

working situation of the beam-column joint as if it was a part of frame structure, where the beam end is considered as the point of contraflexure and rollers are provided near the ends of columns to simulate inflection points in the structure.

In the test, columns of all the specimens were subjected to axial load, which was applied by a servo-controlled hydraulic jack. An electric servo-controlled actuator was employed to apply reversed cyclic load at the beam end. The moment arm for all specimens was 1350 mm from the centerline of the column.

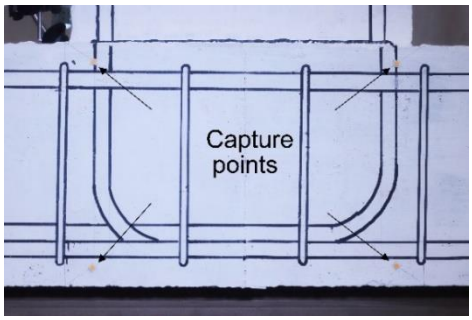

(a) Graphical data capture points on the joint

(b) Vision-Based Sensor Set-up

Fig. 4 Illustration of vision-based sensor for non-contact structural displacement

2.4 Instrumentation

Specimens were instrumented with different types of measuring instruments in this experimental study. As shown in Fig. 3, strain gauges were attached in various locations to monitor the strain variation of longitudinal and transverse reinforcement bars. One linear variable displacement transducers (LVDT) with a range of 300 mm was installed to measure the lateral displacement of beam end during the experiment. All strain gauges and the LVDT were connected to the data acquisition system to record the strain and displacement data during the test. Vision-Based Sensors for Non-Contact Structure Displacement Measurement were adopted to monitor the shear deformation of the beam-column connection region as shown in Fig. 4. By using the digital single-lens reflex camera (DSLR) and a set of capture points installed at the four corners within the joint core, the photographic data was recorded and the shear deformation of joint was found by using a MATLAB algorithm.

2.5 Test procedure

Firstly, axial load was applied to the end of the column by the hydraulic actuator, which was equivalent to 10% of the axial capacity of the column and maintained constant during the test to simulate the gravity load from upper floors. To simulate the displacement reversal of beam-column joints during earthquake actions, the specimens were subjected to reversed cyclic lateral displacement which applied each target displacement in a quasi-static manner by the electric actuator. The cyclic loading was predetermined in terms of storey drift ratios, where the storey drift ratio Δ

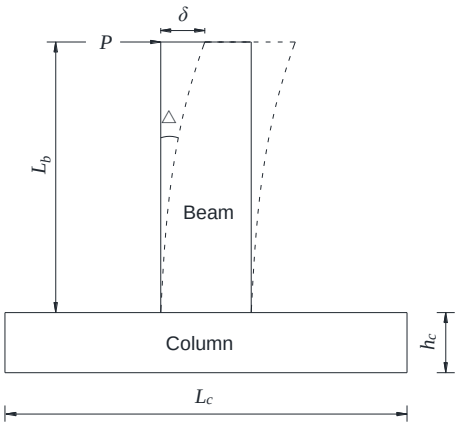

Fig. 5 Storey drift ratio

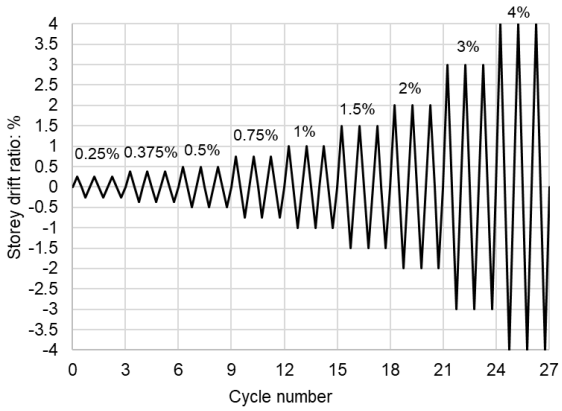

Fig. 6 Loading history

is defined as (Fig. 5)

$$\Delta = \frac{\delta}{L_b + 0.5h_c} \times 100\% \quad (1)$$

where δ is the displacement at the level of cyclic loading; L_b and h_c are the beam length and the depth of the column, respectively.

A typical lateral displacement history consisting of three cycles at monotonically increasing drift levels (0.25%, 0.375%, 0.5%, 0.75%, 1.0%, 1.5%, 2.0%, 3.0%, and 4.0%), as shown in Fig. 6, was used for all specimens until the restoring force is reduced to 80% of the peak load, when the specimen was assumed to have failed.

3. Test results and discussion

3.1 General test observations

Fig. 7 shows the progressive crack pattern and the failure mode of specimen E00. In the initial stage of 0.25% drift ratio, small amount of flexural cracks developed at the critical region of the beam which were parallel to the transverse reinforcement. Extensive flexural cracks formed in beam at 0.5% drift ratio. At the same time, fine vertical cracks around the joint region were found, which was caused by bond-slip behavior of steel bars. Diagonal shear cracks occurred in the joint region when the drift ratio was up to 1% and side cracks at the beam-column connection could be observed. As the drift ratio increased, the width and number of the cracks increased. When the drift ratio reached 4%, visible crushing and spalling of concrete in the joint region could be observed. Concrete expanded laterally and the damage pattern on both sides of the joint (sides A and B) was symmetrical. Joint shear failure was observed, and the critical region of beam cracked extensively due to the formation of a plastic hinge.

Fig. 8 shows the progressive crack pattern and failure mode of specimen E37. The propagation of cracks was similar to specimen E00, whereas the width and number of the cracks in the beam are significantly less than that of specimen E00. It can also be observed that the damage on the eccentric side (side B) was more severe than that of the other side (side A).

Fig. 9 shows the progressive crack pattern and failure mode of specimen E75. Similar to other specimens, fine and horizontal flexural cracks developed when the drift ratio

(a) 0.25% drift ratio

(b) 0.5% drift ratio

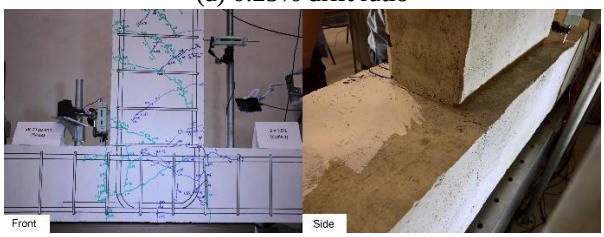

(c) 1.0% drift ratio

(d) 4.0% drift ratio

Fig. 7 Crack patterns of specimen E00

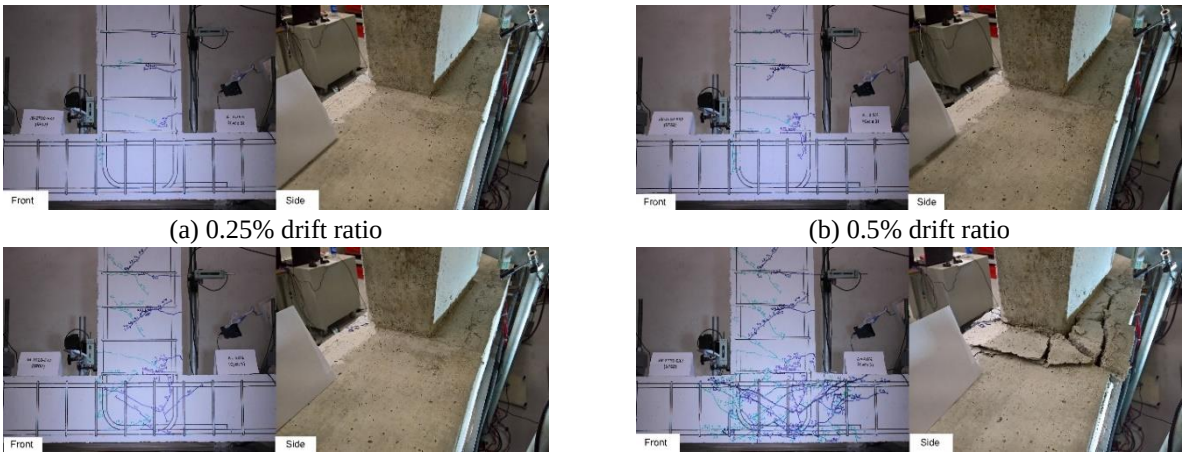

(a) 0.25% drift ratio (b) 0.5% drift ratio

(c) 1.0% drift ratio (d) 4.0% drift ratio

Fig. 8 Crack patterns of specimen E37

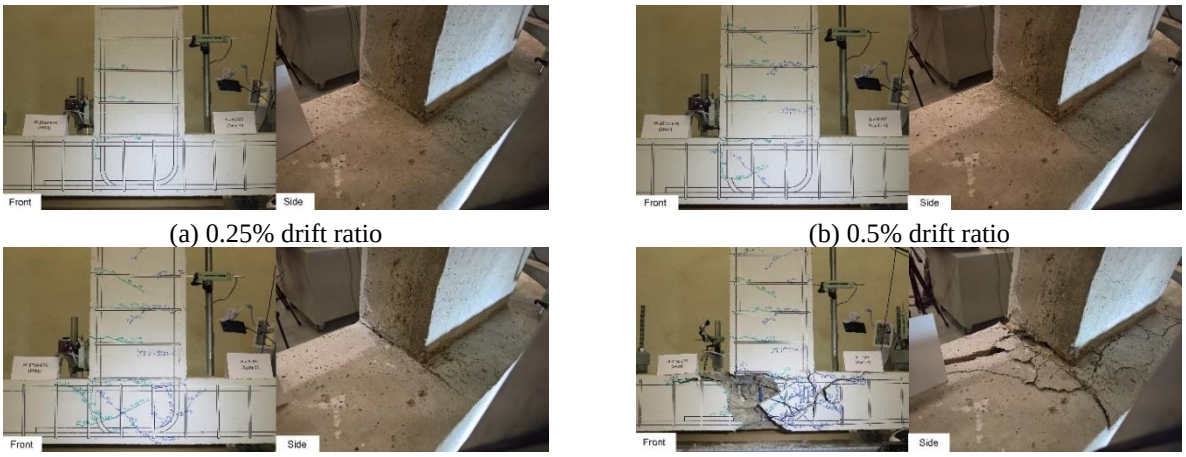

(a) 0.25% drift ratio (b) 0.5% drift ratio

(c) 1.0% drift ratio (d) 4.0% drift ratio

Fig. 9 Crack patterns of specimen E75

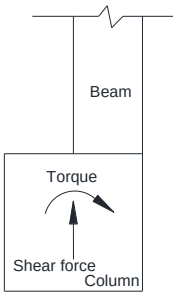

Fig. 10 Torsional moment of the joint core

was 0.5%, a number of diagonal shear cracks were found in the joint region, as can be seen from Fig. 9(b). After three cycles of 1% drift ratio, the diagonal cracks extended while the flexure cracks on the beam stop growing. Visible crushing and spalling of concrete in the joint region were observed after 3% drift ratio, which indicates that the failure of specimen E75 is earlier than that of other joints. Strength degradation was attributed to the crushing of concrete, followed by the beam bars losing its bond and anchorage within the joint region. As shown in Fig. 9(d), the joint was subjected to shear failure, and the beam-column joint was seriously damaged but the flexural cracks on the beam showed no significant propagation. It was also found that concrete on the eccentric side (side B) has seriously damaged while concrete on the other side (side A) maintained its integrity. This may be arisen from the combination effect of shear force and torsional moment for eccentric beam-column joints, as indicated in Fig. 10. The pre-mature shear failure of joint did not satisfy the seismic resistance criteria.

3.2 Hysteretic behavior and damage characteristics

Fig. 11 illustrates the hysteretic responses of test specimens, which can show the effect of eccentricity on the joint behavior in terms of strength degradations, failure mode (BJ-failure mode: joint shear failure after beam yielding; J-failure mode: joint shear failure), and displacement ductility. The lateral load-displacement envelopes of test specimens are presented in Fig. 12. The displacement ductility factor, μ, and the shear force in the joints can be calculated by Eqs. (2)-(3) (Kuang and Wong 2006), respectively.

$$\mu = \frac{\Delta_u}{\Delta_y} \tag{2}$$

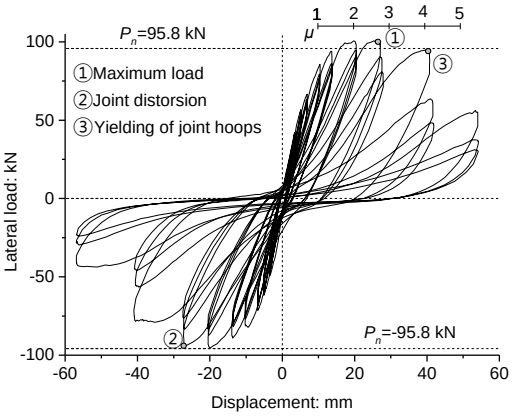

(a) Specimen E00

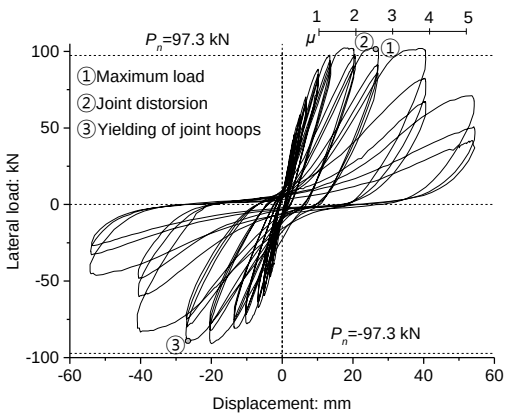

(b) Specimen E37

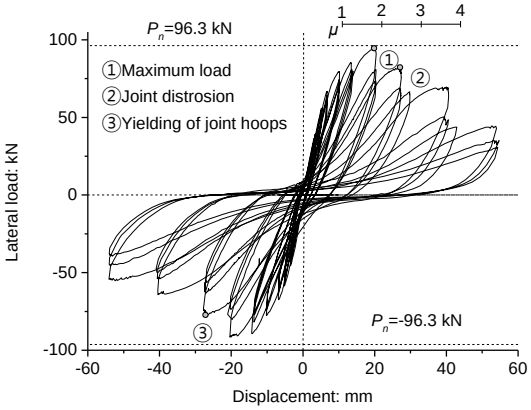

(c) Specimen E75

Fig. 11 Lateral load-displacement response of test specimens

Table 2 Experimental results

Specimen		E00	E37	E75
Yield Displacement Δ_y: mm		9.84	10.41	10.99
Nominal Load Capacity of Beam P_n: kN		95.83	97.25	96.36
Maximum Load P_{max}: kN		100.64	102.39	94.13
Initial Stiffness K: kN/mm		9.74	9.34	8.76
Ductility Ratio μ		4.59	4.62	3.10
Maximum Joint Shear V_j: kN		255.85	260.29	239.30
P_{max}/P_n		1.05	1.05	0.98
Normalised joint shear stress	$\upsilon/\sqrt{f'_c}$	0.50	0.47	0.46
	Relative value to E00	1.00	0.94	0.91
Failure Mode		BJ	BJ	J

$$V_J = T_b - V_{col} = \frac{PL_b}{0.9d_b} - \frac{p\left(L_b + 0.5h_c\right)}{L_c} \tag{3}$$

where Δ_y is the yield displacement shown in Fig. 13. It was determined by extrapolation from measured displacement at $0.75P_n$, and Δ_u is ultimate displacement corresponding to the loss of 20% of the maximum lateral load of the test specimen; V_j is the shear force in the beam-column joint; T_b and V_{col} are the tensile force in steel of the beam and the shear force of the column, respectively; P is the applied lateral load at the end of beam; d_b and L_c are the effective depth of beam and the length of column, respectively. The calculated results were shown in Table 2.

As indicated in Table 2 and Fig. 11, for specimens E00 and E37, the maximum applied load is larger than the beam nominal load capacity and P_{max}/P_n of both specimens is larger than 1.0, where the load P_n is the reversed-cyclic applied load when the beam reaches its ultimate flexural strength. The value of the ultimate flexural strength was determined based on the code-specified rectangular stress block for concrete at the ultimate limit state without incorporating any partial factors of safety. The result indicates that the beam yielded before joint shear failure for the two specimens. However, for specimen E75, P_{max}/P_n is smaller than 1.0 which means that the joint is subject to shear failure before beam yielding. Moreover, the normalised joint shear stress decreases from 0.5 to 0.46 with the increase of eccentricity. This indicates that eccentricity weakened the joint and shift the failure mode from BJ mode to J mode.

Table 2 shows that the specimens E37 and E75 have lower initial stiffness comparing to that of specimen E00 by 4.1% and 10.1%, respectively. From the hysteretic responses of all three specimens, as shown in Fig. 11, the maximum load occurred at 2% storey drift ratio for specimens E00 and E37, but it was at 1.5% drift ratio for specimen E75. It can be seen from Fig. 12 that the seismic performance of specimen E75 is significantly different from those of the other two specimens. The maximum lateral force of specimen E75 was also lower than those of Specimens E00 and E37. The maximum joint shear strength

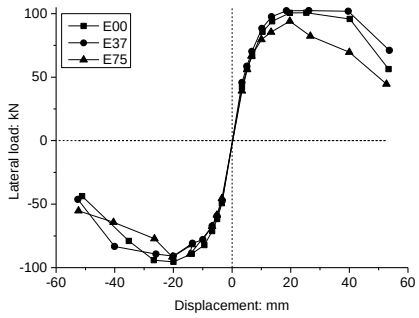

Fig. 12 Envelopes of lateral load-displacement

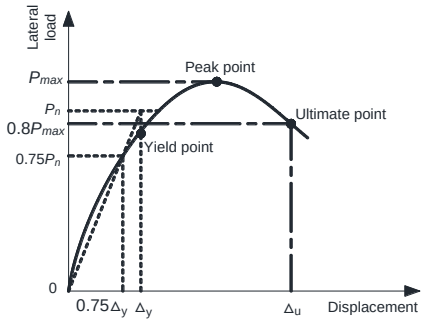

Fig. 13 Characteristic points on load-displacement curve

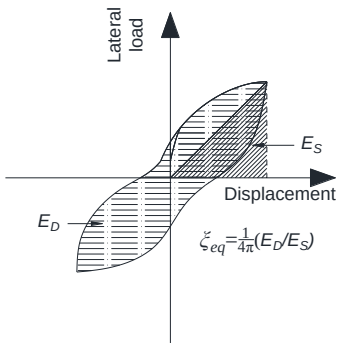

Fig. 14 Normalized index for energy dissipation capacity

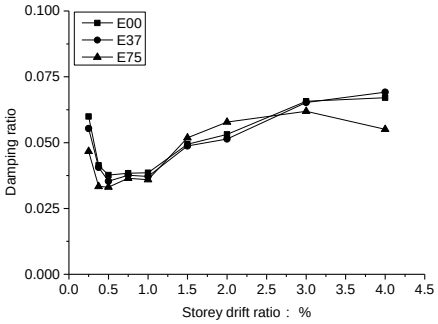

Fig. 15 Equivalent damping ratio of test specimens

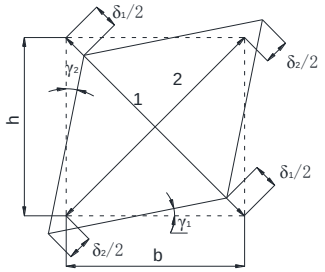

Fig. 16 Evaluation of shear deformation in joint regions

and ductility of the specimen E75 reduced by 6.7% and 32.5% compared to those of the specimen E00. For specimen E75, the significant drop in bearing capacity occurred after 1.5% drift ratio, while it occurred after 3% drift ratio for specimens E00 and E37. The major joint failure was identified after 2% drift ratio for specimen E75, but it was after 3% drift ratio for specimens of E00 and E37. Eventually, the lateral load-displacement responses for all the specimens exhibited significant pinching behavior, which was the typical response of the shear or bond-slip mechanism.

Note that the shear strength and ductility of specimen E37 were similar to specimen E00. This revealed that the $b_c/8$ eccentricity has minimal effect on the seismic performance of the beam-column joints in this particular study.

3.3 Damping ratio

The equivalent viscous damping ratio ξ_{eq}, as shown in Fig. 15, was used to evaluate the energy dissipation capacities of the test specimens. The quantitative index ξ_{eq} represents the effect of hysteretic damping with respect to an equivalent linear elastic system on the energy dissipation capacity, which can be defined as

$$\xi_{eq} = \frac{1}{4\pi}\frac{E_D}{E_S} \tag{4}$$

where E_D is the energy dissipated per cycle, as shown in Fig. 14, and E_S is defined as the elastic strain energy.

Fig. 15 describes the energy dissipation capacity of the specimens. Specimen E37 with an eccentricity of $b_c/8$ had a slight influence in this study as the observed equivalent viscous damping ratio is similar to the specimen E00. However, the large eccentricity of $b_c/4$ had significant adverse effects on the seismic performance of specimen E75.

3.4 Shear deformation of joints

The shear deformation of the beam-column joint panel can be estimated by the shear angle, γ, which is calculated by

$$\gamma = \frac{\sqrt{b^2+h^2}}{2bh}(\delta_1+\delta_2) \tag{5}$$

where δ_1 and δ_2 are the changes of diagonal lengths of joint measured by the digital single-lens reflex camera; b and h are the width and height of the joint, respectively (Fig. 16).

Fig. 17 illustrates the shear deformation of specimens and the missing data due to concrete spalling in the joint region. For specimen E00, as shown in Fig. 17(a), side B and side A show the similar joint shear deformation during the experiment, which implies that the concrete on both sides was evenly contributed to the shear resistance of the joint and the specimen had no torque in the joint core. As

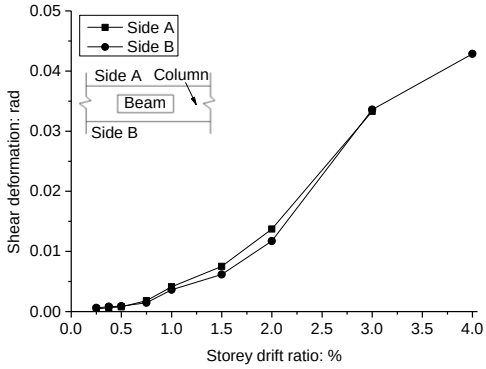

(a) Specimen E00

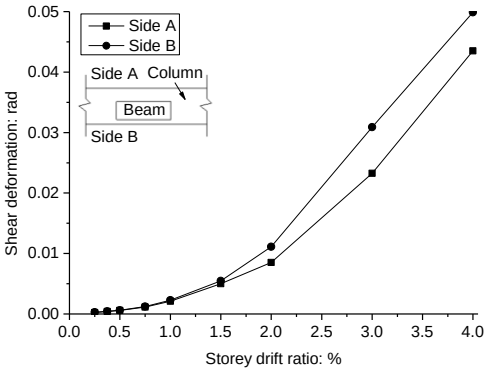

(b) Specimen E37

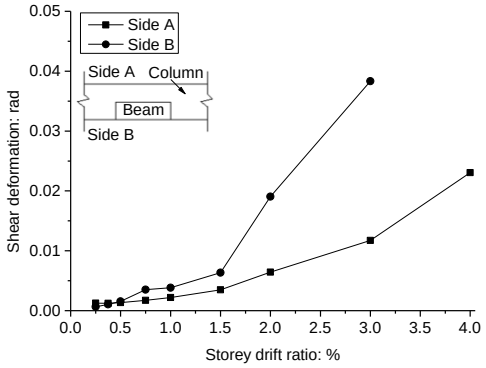

(c) Specimen E75

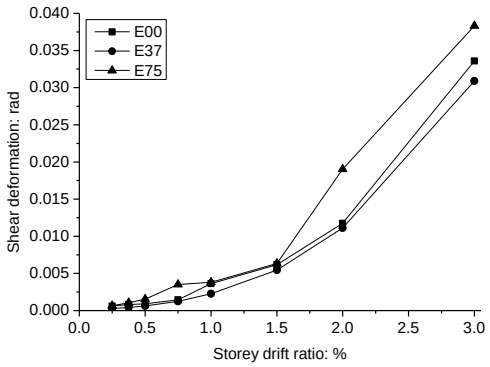

(d) Shear deformation for all specimens of the side B

Fig. 17 Shear deformation in joint core

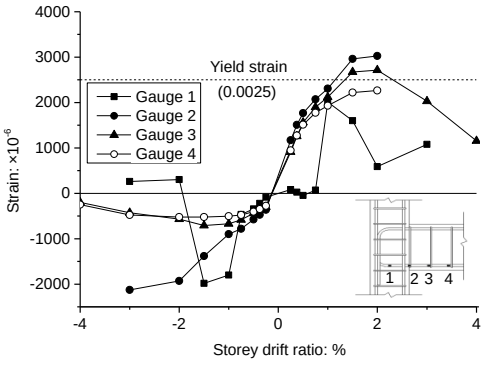

(a) Specimen E00

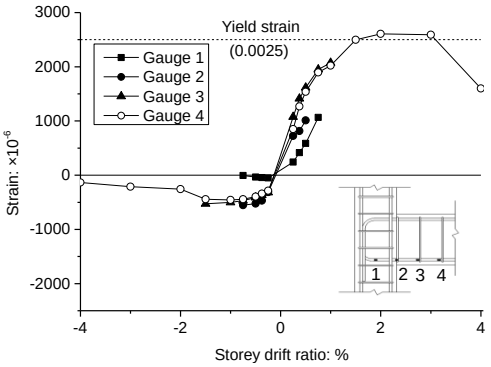

(b) Specimen E37

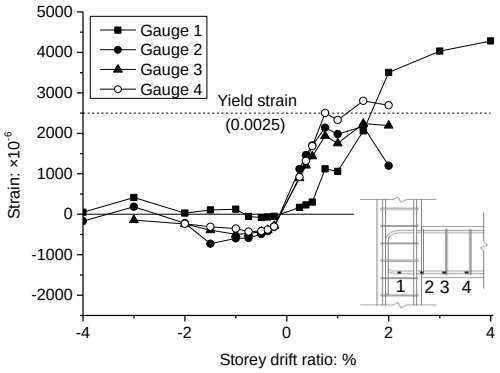

(c) Specimen E75

Fig. 18 Strain profiles of longitudinal reinforcement of beams

can be seen from Fig. 17(b) for the specimen E37 and Fig. 17(c) for specimen E75, respectively, the shear deformation of side B is greater than that of the side A. More specifically, the joint panel of side B was subjected to

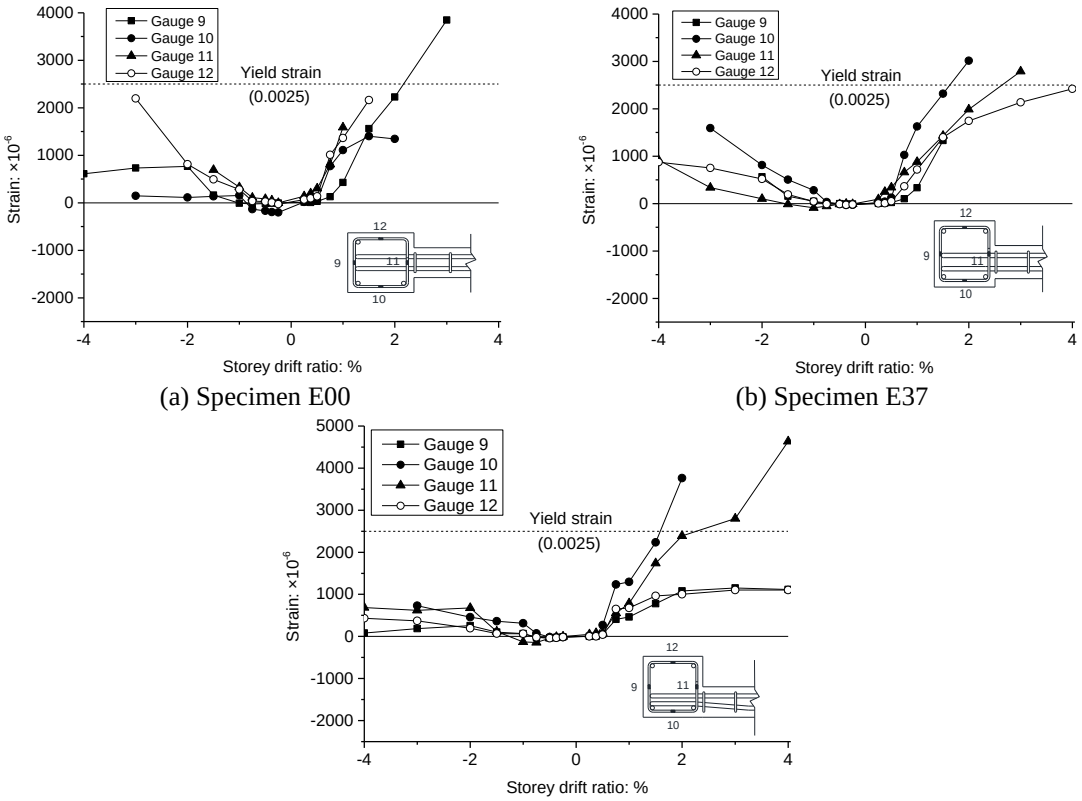

(a) Specimen E00

(b) Specimen E37

(c) Specimen E75

Fig. 19 Strain profiles of joint hoops

significantly higher shear deformation for the eccentric specimen E75, which indicates that the eccentric side (side B) of joint would fail first with the increase of eccentricity.

Fig. 17(d) shows the comparison of shear deformation on the eccentric side of the three specimens. It can be observed that the shear deformation of specimen E00 and specimen E37 is almost similar, while the shear deformation of specimen E75 is significantly higher. This further shows that the small eccentricity has little effect on the shear strength of the non-seismically designed beam-column joints, but when it increases to $b_c/4$, the seismic performance of eccentric joint decreases significantly.

For eccentric joints, the eccentricity of the tensile force of steel bars and concrete compression transferred of the beam generates the torque. The shear force generated by the torque is in the same direction of joint shear applied on the eccentric side (side B) but opposite to the other side (side A). The damage to the eccentric side is thus more severe than the other side, which has been verified by the crack patterns as mentioned. With the increase of eccentricity, it leads to more serious damage on joints of the specimens. The effect of torque may be treated in terms of reduction of the effective shear area within the joint which resulted in the decrease of shear capacity.

3.5 Strain profiles of reinforcement

The strain of the flexural reinforcement and the stirrups in the joints are shown in Fig. 18 and Fig. 19, respectively. The yield strain is 0.0025 mm/mm for all steel bars in this experiment, and the missing test results mainly due to the failure of strain gauge after yielding of reinforcements.

Figs. 18(a)-(b) show that flexural reinforcing bars yielded at the end of the beam near the joint when the storey drift ratio reached at around 1.5%, for specimens E00 and E37. In specimen E75 (Fig. 18(c)), however, the longitudinal bar inside the beam-column joint (Gauge 1) yielded until the drift ratio reached 2%, and the strain was significantly larger than others within the beam of this specimen, which is caused by the loose of bonding due to major cracks and spalling of concrete within the joint core. This comparison confirmed that the beam-column joints failed after the formation of plastic hinges at the end of the beam for specimens E00 and E37, while the failure of joint occurred when the beam just yielded before well development of plastic hinges for specimen E75.

As shown in Fig. 19, it can be observed that the joint stirrups yielded when the storey drift ratio reached around 2%. In this stage, significant diagonal cracks developed in the joint and they were clearly shown in Figs. 7-9. Moreover, by comparing the strains of gauge 10 on side B and that of gauge 12 on side A, the uneven strain development for the specimens was observed. Specimen E00 with no eccentricity shows a similar strain distribution for both strain gauges 10 and 12. Fig. 19(b) shows the gauge 10 in specimen E37 yielded at the drift ratio of 2%, while the maximum strain of gauge 12 was 0.002422 mm/mm, which was close to the yield strain. In specimen E75, the maximum strain of gauge 12 was 0.001103 mm/mm, which was far less than the yield strain while that

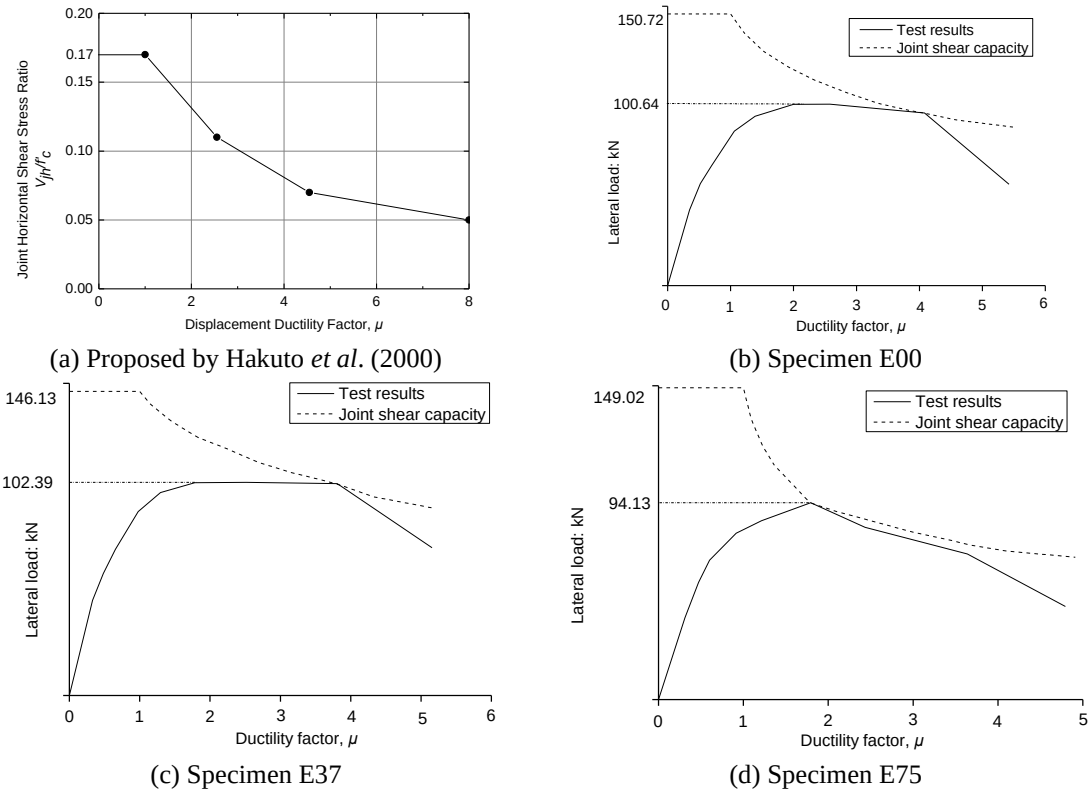

(a) Proposed by Hakuto *et al*. (2000) (b) Specimen E00

(c) Specimen E37 (d) Specimen E75

Fig. 20 Degradation of joint shear strength

Table 3 Normalised shear stress and the ductility ratio of joints with different eccentricity

Specimen		*e*: mm	e/b_c	Ductility Ratio		Normalised joint shear strength	
				μ	Relative value	$v/\sqrt{f'_c}$	Relative value
This research	E00	0	0	4.59	1.00	0.50	1.00
	E37	37	0.125	4.62	1.01	0.47	0.94
	E75	75	0.25	3.10	0.68	0.46	0.91
Lee and Ko (2007)	W0	0	0	4.58	1.00	0.80	1.00
	W75	75	0.125	4.61	1.01	0.79	0.98
	W150	150	0.25	3.41	0.74	0.76	0.95

of gauge 10 had reached the yield strain when the drift ratio was 2%. On side A, the strains of gauge 12 in eccentric specimens were less than those in specimen E00 due to the cancellation effect of shear stresses and torque which counteract each other. These results confirm the observations of more extensive shear or torsion cracks on side B of the eccentric connections.

3.6 Degradation of joint shear capacity

Previous studies (Park and Paulay 1975, Zhang and Jirsa 1982, Park 1997, Hakuto *et al*. 2000) have shown that the shear strength of RC beam-column joints decreases with the formation of plastic hinge in the adjacent beam. It is caused by the effect of the loss of bond strength and yield penetration of reinforcement from the plastic hinges of the adjacent beam. The empirical model has been proposed based on the experimental results, as shown in Fig. 20(a) (Hakuto *et al*. 2000). According to the test results in this study, the conceptual model for the degradation of joint shear capacity is shown in Figs. 20(b)-(d). The solid lines are reproduced from the positive envelope of the hysteretic curves of the tested specimens and the dotted lines represent the joint shear capacity.

For specimen E00, E37, and E75, according to HKSUC 2013, the values of lateral load derived from joint shear capacity are 150.72 kN, 146.13 kN, and 149.02 kN, respectively. The conceptual model for joint shear deterioration of three specimens were presented in Fig. 20. Without considering the effect of eccentricity, the failure mode of specimen E75 is the same as that of specimens E00 and E37 i.e., joint shear failure after beam yielding. However, it has been shown that joint shear failure occurred when the beam just yielded for specimen E75, which indicates that when the eccentricity reaches $b_c/8$, it has a negative effect on the joint shear capacity and the value is largely reduced from 149.02 kN to 94.14 kN, which is equivalent to 36% of the original strength.

In order to further verify the effect of joint eccentricity, the experimental results of Lee and Ko (2007) are used as

reference. They have performed cyclic tests on RC exterior beam-column joints with increasing eccentricity. For the convenience of analysis, the relative normalised shear stress and the ductility ratio of joints with different eccentricity are shown in Table 3.

The effects of eccentricity are evident. The small eccentricity of $b_c/8$ has minimal influence, while larger eccentricity of $b_c/4$ has significant detrimental effects on the seismic performance of joints. The experimental results in this study aligned with those from other researchers.

4. Comparison the predictions of design codes

By comparing the experimental results with the predicted values of three seismic design codes (ACI 318-14, NZS 3101:2006 and Eurocode 8) and two non-seismic design codes (HK code and Eurocode 2), the reliability of existing codes in predicting the shear strength of the exterior beam-column joints with the non-seismic design under reversed cyclic loading is evaluated.

4.1 ACI 318-14

In ACI 318-14, the exterior beam-column joint shear strength for normalweight concrete is specified below

$$V_j = 0.85\sqrt{f_c^{'}}A_j \tag{6}$$

where f_c' is the compressive cylinder strength of concrete, A_j is the effective cross-sectional area within a joint, which is computed from joint depth times effective joint width. After removing the strength reduction factor of 0.85, the shear strength of exterior joint shall be rewritten as

$$V_j = \sqrt{f_c^{'}}A_j \tag{7}$$

4.2 NZS 3101

From NZS 3101:2006 (2017), the shear strength across a joint for exterior joints can be derived from the code provision and rearranges to the following equation

$$V_j = \frac{1}{6}A_{jh}f_c^{'}b_j h_c\left(\frac{\beta f_y A_s}{f_{yh}}\right)^{-1}\left(0.7-\frac{C_j N_o^*}{f_c^{'}A_g}\right)^{-1} \tag{8}$$

where A_{jh} is the area of total horizontal joint shear reinforcement; f_c' is compressive cylinder strength of concrete. The effective width b_j is usually taken as the smaller of b_c or $b_w+0.5h_c$, when $b_c \geq b_w$, nevertheless it is not exceeding $0.5(b_w+b_c+0.5h_c)-e$ for eccentric beam column joints with ductile, where e is the eccentricity between the centrelines of the column and beam at a joint; h_c is the overall depth of column; β is the ratio of compression beam reinforcement area to tension beam reinforcement area; N_o^* is the axial column load; A_s and A_g are area of tension beam reinforcement and gross area of column section, respectively.

4.3 Eurocode 8

The horizontal shear strength acting on the joint core in Eurocode 8: Part 1 for exterior beam column joints providing horizontal links can be calculated by

$$V_j = \left[\left(\frac{A_{sh}f_y}{b_j h_{jw}}+f_{ctd}\right)\left(f_{ctd}+\upsilon_d f_c^{'}\right)\right]^{0.5}\times b_j h_{jc} \tag{9}$$

where f_c' is the compressive cylinder strength of concrete; b_j is the effective joint width; A_{sh} is the total area of the horizontal links; f_{ctd} is the tensile strength of concrete; υ_d is the design axial force of the column; and h_{jw} and h_{jc} are the distance between the top and the bottom reinforcement of the beam and the distance between extreme layers of column reinforcement, respectively.

4.4 Hong Kong code

In Hong Kong code: Code of Practice for Structural Use of Concrete 2013, the shear strength can be derived from the code provision and calculated by

$$V_j = \frac{A_j f_y}{0.5-\dfrac{C_j N}{0.8A_c f_{cu}}} \tag{10}$$

where A_j is the area of effective horizontal joint shear reinforcement; C_j=1 if joint has beams in one direction only; N is the design axial column load; and A_c is the area of column section; f_{cu} is the compressive cube strength of concrete.

4.5 Eurocode 2

In Eurocode 2, there is no provision for design of beam-column joint. Considering beam-column joint as a part of the column (Parker and Bullman 1997), the shear strength is calculated according to Eurocode 2: Design of concrete structures-Part 1-1: Section 6.2 as follows

$$V_j = \left[C_{R,c}k\left(100\rho_1 f_c^{'}\right)^{1/3}+1.5k_1\sigma_{cp}\right]b_w d+0.9df_y A_{sw}/s \tag{11}$$

where $C_{R,c}$ is the shear strength of concrete; $k=(1+\sqrt{(200/\mathrm{d})}\leq 2.0)$ with d in mm; ρ_1 is the tensile reinforcement ratio, and it is not greater than 0.02; f_c' is the compressive cylinder strength of concrete in MPa; the recommended value of k_1 is 0.15; σ_{cp} is the axial stress of column due to axial loading, which is not greater than 0.2 times of concrete compressive strength; A_{sw} is cross-sectional area of the shear reinforcement and s is the spacing of hoops. b_w is the width of section and d is the effective depth of the section. In the calculation of this study, the partial factor of 1.5 for concrete is not considered (Parker and Bullman 1997).

4.6 Comparison of experimental results to codes' predictions

Table 4 shows the comparison of experimental results to predictions from three seismic codes and two non-seismic

Table 4 Experimental shear strength and comparisons with different codes

Specimen	Experimental shear strength V_{exp}: kN	Seismic design codes			Non-seismic design codes	
		V_{exp}/V_{ACI}	V_{exp}/V_{Nzs}	V_{exp}/V_{EC8}	V_{exp}/V_{HK}	V_{exp}/V_{EC2}
E00	255.85	0.50	0.65	0.96	0.67	1.03
E37	260.29	0.47	0.66	0.93	0.70	1.04
E75	239.30	0.46	0.77	0.88	0.63	0.96

codes of practice.

It can be seen from Table 4 that all seismic design codes overestimated the shear strength of the joints. For ACI 318 and Eurocode 8, with the increase of eccentricity, the extent of overestimation of the shear strength of joints by the codes becomes more inaccurate. The three seismic codes above are not recommended to predict the seismic performance of beam-column joints with non-seismic design, especially eccentric joints.

In the two non-seismic design codes, Eurocode 2 has better predictions for the seismic performance of the joints when comparing to that of the Hong Kong Code of Practice. However, with the increase of eccentricity, Eurocode 2 underestimated the shear strength of joint, which indicates that eccentricity cannot be well addressed by the code of practice.

5. Conclusions

Three non-seismically designed eccentric RC beam-column joints were tested in this study. Based on the evaluation of the reversed cyclic loading responses of the joints in this experimental investigation and other relevant report, the following conclusions are drawn.

(a) The joint without eccentricity presented better seismic performance with limited ductility and moderate strength degradation after flexural yielding. With increase of eccentricity, the following behaviors were observed: 1.) the magnitude and ability for energy dissipation are weakened and reduced; 2.) more severe concrete spalling in the joint region; 3.) reduced equivalent viscous damping ratio; 4.) more severe joint shear deformation in the joint. The eccentricity between beam and column centerlines has detrimental effects on the seismic performance of the joints. The small eccentricity of $b_c/8$ has minimal influence. Obviously, significant reductions in stiffness, shear capacity, and ductility were found when the eccentricity increased to $b_c/4$. Similar findings have also been observed from other researcher's study.

(b) The eccentricity caused uneven strain distribution across the joint stirrups within the joint region. The strain of the leg located close to the eccentric side is larger than that on the side far away from the eccentricity. With higher eccentricity, the development of strain in the leg on the eccentric side grows in proportion. The traditional assumption for equal strain across the section should be further reviewed and studied.

(c) The failure mode of joint with eccentricity was shifted to brittle mode (joint shear failure for the specimen E75) from ductile mode (joint shear failure after beam flexural yielding in the specimens E37 and E00) for those with small or without eccentricity. There is an urgent need to review and retrofit non-seismically designed eccentric beam-column joints in existing RC frames that have an eccentricity of $b_c/4$ or larger.

(d) The three seismic design codes of practice and the Hong Kong code of practice overestimated the shear strength of the non-seismically designed beam-column joints to different extents. Eurocode 2, however, has a relatively good prediction of joint shear strength. Nevertheless, eccentricity reduces its reliability. Therefore, it is necessary to establish a rational method to analyze the seismic performance of eccentric RC beam-column joints in low to moderate earthquake areas.

Acknowledgments

The work described in this paper was fully supported by a grant from the Research Grants Council of the Hong Kong Special Administrative Region, China (Project No. UGC/FDS25/E08/17).

References

ACI (2014), Building Code Requirements for Structural Concrete, American Concrete Institute, Farmington Hills, MI, USA.

Al-Osta, M.A., Khan, M.I., Bahraq, A.A. and Xu, S.Y. (2020), "Application of ultra-high performance fiber reinforced concrete for retrofitting the damaged exterior reinforced concrete beam-column joints", *Earthq. Struct.*, **19**(5), 361-377. http://doi.org/10.12989/eas.2020.19.5.361.

Basha, A.M. and Fayed, S. (2019), "Behavior of RC eccentric corner beam-column joint under cyclic loading: an experimental work", *Civil Eng. J.*, **5**(2), 295-308. https://doi.org/10.28991/cej-2019-03091245.

Building Department (2013), Code of Practice for Structural Use of Concrete 2013, Building Department, Mongkok, Kowloon, Hong Kong.

Choi, K.K., Dinh, N.H. and Kim, J.C. (2017), "Behaviour of non-seismic detailed reinforced-concrete beam-column connections", *P. I. Civil Eng-Struct. B.*, **170**(SB7), 504-520. https://doi.org/10.1680/jstbu.16.00201.

EERI (1991), The Newcastle, Australia Earthquake, Earthquake Engineering Field Investigation Team, Institution of Structural Engineers, UK.

EERI (Earthquake Engineering Research Institute) (2001), "Chi-Chi, Taiwan, Earthquake of September 21, 1999", Report No. 02/2001, Earthquake Engineering Research Institute, Oakland, America.

Eurocode (2013), Design of Structures for Earthquake Resistance-Part 1: General Rules, Seismic Actions and Rules for Buildings, European Committee for Standardization, Brussels, Belgium.

Eurocode (2014), Design of Concrete Structures-Part1-1: General Rules and Rules for Buildings, European Committee for Standardization, Brussels, Belgium.

GEO (Geotechnical Engineering Office) (2015), "Seismicity of Hong Kong (GEO information Note 08/2015)", 1-5.

Hakuto, S., Park, R. and Tanaka, H. (2000), "Seismic load tests on interior and exterior beam-column joints with substandard reinforcing details", *ACI Struct. J.*, **97**(1), 11-25. https://doi.org/10.14359/829.

Halahla, A.M., Rahman, M.K., Al-Gadhib, A.H., Al-Osta, M.A. and Baluch, M.H. (2019), "Experimental investigations and FE simulation of exterior BCJs retrofitted with CFRP fabric", *Earthq. Struct.*, **17**(4), 337-354. http://doi.org/10.12989/eas.2019.17.4.337.

Kaplan, H., Bilgin, H., Yilmaz, S., Binici, H. and Oztas, A. (2010), "Structural damages of L'Aquila (Italy) earthquake", *Nat. Hazard. Earth Syst. Sci.*, **10**(3), 499-507. https://doi.org/10.5194/nhess-10-499-2010.

Karayannis, C.G. and Golias, E. (2021), "Strengthening of deficient RC joints with diagonally placed external C-FRP ropes", *Earthq. Struct.*, **20**(1), 123-132. http://doi.org/10.12989/eas.2021.20.1.123.

Kuang, J.S. and Wong, H.F. (2006), "Effects of beam bar anchorage on beam-column joint behaviour", *P. I. Civil Eng-Struct. B.*, **159**(2), 115-124. https://doi.org/10.1680/stbu.2006.159.2.115.

Kuang, J.S. and Wong, H.F. (2013), "Horizontal hoops in non-seismically designed beam column joints", *HKIE Tran.*, **20**(3), 164-171. https://doi.org/10.1080/1023697x.2013.812388.

Kwon, G.J., Park, J.W., Yoon, S.G., Kim, T.J. and Lee, J.Y. (2012), "Behavior of reinforced concrete inclined column-beam joints", *J. Korea Concrete Inst.*, **24**(2), 147-156. https://doi.org/10.4334/JKCI.2012.24.2.147.

Lee, H.J. and Ko, J.W. (2007), "Eccentric reinforced concrete beam-column connections subjected to cyclic loading in principal directions", *ACI Struct. J.*, **104**(4), 459-467. https://doi.org/10.14359/18776.

Lee, J.Y., Kim, J.Y. and Oh, G.J. (2009), "Strength deterioration of reinforced concrete beam-column joints subjected to cyclic loading", *Eng. Struct.*, **31**(9), 2070-2085. https://doi.org/10.1016/j.engstruct.2009.03.009.

Marthong, C. (2019), "Behavior of repaired RAC beam-column joints using steel welded wire mesh jacketed with cement mortar", *Adv. Concrete Constr.*, **8**(2), 91-100. http://doi.org/10.12989/acc.2019.8.2.091.

Mirzabagheri, S., Tasnimi, A.A. and Issa, F. (2018), "Experimental and numerical study of RC interior wide beam-column joints subjected to lateral load", *Can. J. Civil Eng.*, **45**(11), 947-957. https://doi.org/10.1139/cjce-2018-0049.

Moehle, J.P. and Mahin, S.A. (1991), "Observations on the behavior of reinforced concrete buildings during earthquakes", *ACI Spec. Publ.*, **127**, 67-90,

Mogili, S., Kuang, J.S. and Huang, Y.C (2019), "Effects of beam-column geometry and eccentricity on seismic behaviour of RC beam-column knee joints", *Bull. Earthq. Eng.*, **19**(5), 2671-2686. https://doi.org/10.1007/s10518-019-00562-y.

Oinam, R.M., Kumar, P.C.A. and Sahoo, D.R. (2019), "Cyclic performance of steel fiber-reinforced concrete exterior beam-column joints", *Earthq. Struct.*, **16**(5), 533-546. http://doi.org/10.12989/eas.2019.16.5.533.

Park, R. (1997), "A static force-based procedure for the seismic assessment of existing reinforced concrete moment resisting frame", *Bull. N.Z. Nat. Sci. Earthq. Eng.*, **30**(3), 213-226. https://doi.org/10.5459/bnzsee.30.3.213-226.

Park, R. and Paulay, T. (1975), *Reinforced Concrete Structures*, John Wiley and Sons, Inc., New York, USA.

Parker, D.E. and Bullman, P.J.M. (1997), "Shear strength within reinforced concrete beam-column joints", *Struct. Eng.*, **75**(4), 53-57.

Raj, S.D., Ganesan, N. and Abraham, R. (2020), "Role of fibers on the performance of geopolymer concrete exterior beam column joints", *Adv. Concrete Constr.*, **9**(2), 115-123. http://doi.org/10.12989/acc.2020.9.2.115.

Standards New Zealand (2017), Concrete Structure Standard-Incorporating Amendment No. 1, 2, and 3, Standards New Zealand, Wellington, New Zealand.

Vanlalruata, J. and Marthong, C. (2021), "Behaviour of RC beam-column joint with varying location of construction joints in the column", *Earthq. Struct.*, **20**(1), 29-38. http://doi.org/10.12989/eas.2021.20.1.029.

Zhang, L. and Jirsa, J.O. (1982), "A study of shear behaviour of reinforced concrete beam-column joints", PMFSEL Report No. 82-1, Department of Civil Engineering, University of Texas at Austin, Austin, USA.

KT